# Characteristic analysis of aspheric quasi-optical lens antenna in millimeter-wave radiometer imaging system

Won-Gyum Kim,[1] Nam-Won Moon,[1] Manoj Kumar Singh,[2] Hwang-Kyeom Kim,[3] and Yong-Hoon Kim[1,*]

[1]School of Information and Mechatronics, Gwangju Institute of Science and Technology, No. 123 Cheomdan-gawiro, Buk-Gu, Gwangju 500-712, South Korea

[2]DST-Centre for Interdisciplinary Mathematical Sciences (DST-CIMS), Banaras Hindu University (BHU), Varanasi 221 005, India

[3]Defense Acquisition Program Administration, No. 23 Yongsango-Gil, Yongsan-Dong, Yongsan-Gu, Seoul 140-841, South Korea

*Corresponding author: yhkim@gist.ac.kr

Received 22 October 2012; revised 4 January 2013; accepted 6 January 2013; posted 7 January 2013 (Doc. ID 178435); published 11 February 2013

Quasi-optical imaging systems require low blurring effect and large depth of focus (DOF) to get an acceptable sharpness of the image. To reduce aberration-limited blurring, the aspheric convex plano lenses with an aperture diameter of 350 mm are designed in W-band. We analyzed theoretically and experimentally the millimeter-wave band lens characteristics, such as beam spot size, spatial resolution (SR), and DOF, via $f$-number. It is first used to verify the DOF through $f$-number in the system-level test with the developed W-band radiometer imaging system. We have confirmed that the larger $f$-number of quasi-optical lens leads to a larger DOF but a lower SR. © 2013 Optical Society of America

*OCIS codes:* 040.1240, 080.4225, 110.0110, 220.3630, 280.4991, 350.4010.

## 1. Introduction

Imaging systems have been developed in the millimeter-wave (MMW) region because of, in contrast to a visible imager and infrared, their ability to see through bad weather for surveillance and to penetrate opaque objects such as clothing, polymers, and some building materials for security applications [1–4]. There are two optimum frequency bands for the use in MMW imaging, Q-band (35 GHz band) and W-band (94 GHz band). This is because transmission through the atmosphere is significantly better in these atmospheric windows compared to the other frequencies in MMW region. W-band offers better image quality and spatial resolution (SR), as governed by the diffraction limit, compared to the Q-band. The range of MMW imaging system is generally from meters to kilometers between targets and the sensors. However, there are fewer research results for short-range MMW imaging applications, especially less than hundreds of centimeters. Previous works have demonstrated capacities for obtaining high resolution images at close range [5–8]. The focal plane array (FPA) technology is useful due to the high frame rate of the MMW imaging system at the expense of the cost of large area arrays [9–12]. The image acquisition methods are introduced in many papers using mechanically scanned 1D and 2D FPA. A dielectric lens antenna is a good candidate as quasi-optics for the MMW imaging radiometer system due to its advantages of size, weight, and efficiency compared with a metal reflector antenna [13–17]. The SR, the field of view (FOV), and the

1559-128X/13/061122-10$15.00/0

depth of focus (DOF) are the major parameters for a FPA imaging system. The SR based on Rayleigh criteria depends on $f$-number ($f/\#$) of a lens in a given frequency. FOV is limited by the SR and the number of receivers, but it is also limited by the optical coupling efficiency of a close placed receiver's antennas. The DOF is the variable image distance from a lens to a receiver and it depends on $f/\#$ of a lens. In this paper, we present theoretically and experimentally the relationship between lens characteristics and $f/\#$ for W-band quasi-optical radiometer imaging system at the short range. For verification, we have designed two lenses with the different $f/\#$ and the same aperture size at 94 GHz.

The rest of this paper is organized as follows. Section 2 theoretically describes the characteristics of a quasi-optical lens in a MMW focal plane imaging system. The design of an aspheric quasi-optical lens antenna is presented in Section 3. The characteristics of aspheric quasi-optical lenses are experimentally analyzed in Section 4. The conclusion follows in Section 5.

## 2. Characteristics of Aspheric Quasi-Optical Lens in MMW Imaging System

The schematic of a quasi-optical lens is shown in Fig. 1. The main characteristics of a lens are beam spot size, $d_{\text{blur}}$, the SR, $r_{\text{sp}}$, and the DOF. To explain the lens characteristics, it is suitable to understand the relationship between the characteristics and $f/\#$ of a lens in accordance with Gaussian beam propagation. It is necessary to consider the conjugation ratio depending on magnification of a lens in analyzing the relationship. The Gaussian lens equation is given as follows [18–20]:

$$\frac{1}{S_i}+\frac{1}{S_o}=\frac{1}{F}, \tag{1}$$

where $S_i$, $S_o$, and $F$ are the distance between image plane and lens, distance of object plane from lens, and the focal length of the lens. The expression for the magnification, $M$, of the lens is given as

$$M=\frac{S_i}{S_o}. \tag{2}$$

Combining Eqs. (1) and (2), we get the relation between image distance, focal length, and magnification:

$$S_i=(M+1)F. \tag{3}$$

If the magnification, $M$, is relatively low, the lens is used at the infinite conjugate ratio corresponding to $S_i=F$.

The incoming beam is focused by a lens to obtain a small beam spot, as shown in Fig. 1. The focused beam spot spreads on the image plane because of aberration and diffraction of the lens. And these introduce blurring in the image.

In general, the aberration is caused by the spherical geometry of lens surfaces. The aberration-limited spot size, $d_{ab}$, is determined by multiplying the aberration-limited angle angular blur, $\Delta\Theta_{ab}$, by the image distance $S_i$. The aberration-limited angular blur, based on third-order aberration theory, and aberration-limited spot is given as [18,21]:

$$\Delta\Theta_{ab}=(D/F)^3[n^2-(2n+1)q+(n+2)q^2/n]/[32(n-1)^2], \tag{4}$$

$$d_{ab}=\Delta\Theta_{ab}\cdot S_i, \tag{5}$$

where $D$, $F$, $n$, and $q$ are the diameter, focal length, material refractive index, and shape factor of the lens, respectively. The shape factor $q$ of a lens is given by [21]:

$$q=R_2/(R_2-R_1), \tag{6}$$

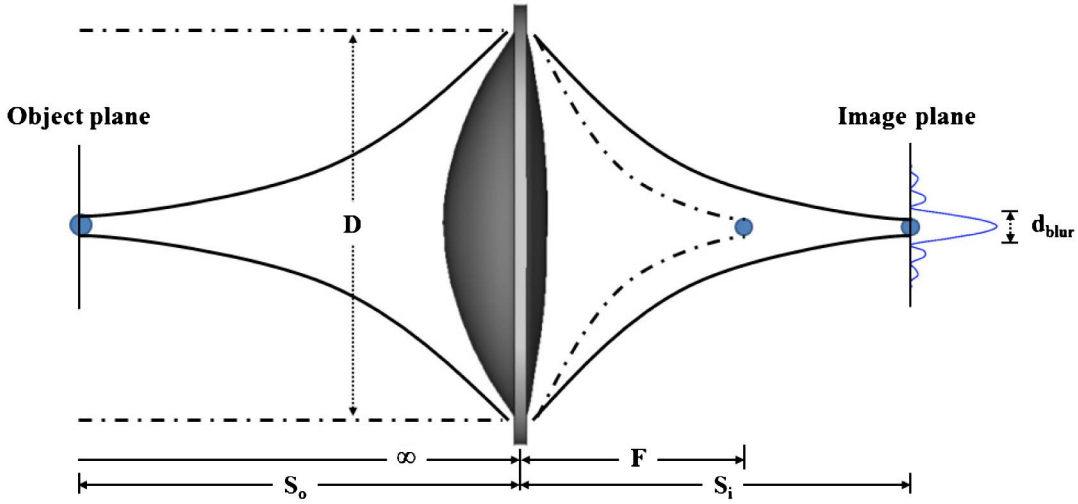


Fig. 1. (Color online) Schematic of quasi-optical lens.

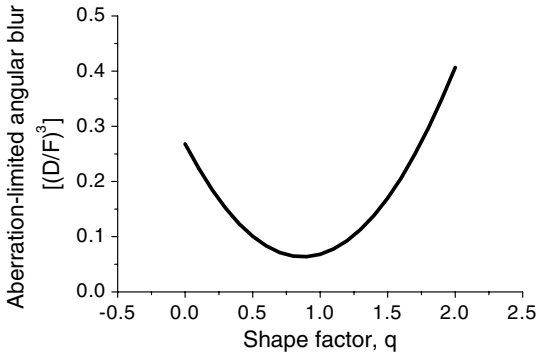


Fig. 2. Aberration-limited angular blur via shape factor.

where $R_1$ and $R_2$ are the radius of curvature for left and right side surface of the lens, as shown in Fig. 1. The variation of the aberration-limited angular blur with shape factor shown in Fig. 2, for the lens made of high-density polyethylene (HDPE) which has a refractive index ($n$) of 1.5187 at 94 GHz [17,20] and it is being operated at the infinite conjugate ratio. An asymmetric shape that corresponds to a $q$-value of about 0.87 is the best singlet shape. It is important to note that the best-form shape of lens is dependent on the refractive index. In case of a typical dielectric singlet, the convex plano shape ($q = 1$), with convex side toward the infinite conjugate, performs nearly as well as the best-form lens. Equation (5) is simplified to Eq. (7) for a spherical convex plano lens in the case of HDPE and the finite conjugate ratio:

$$d_{ab\_\mathrm{HDPE}} = \frac{0.068}{(M+1)^2}\frac{F}{(f/\#)^3}, \tag{7}$$

where $f/\# = F/D$ denotes the $f$-number of the lens.

The diffraction accounts for the spreading of the radiation as it passes through an aperture. Thus, a point object is never imaged on a point in the image plane as shown in Fig. 3(a). The irradiance distribution in the image plane and its cross section is shown in Figs. 3(b) and 3(c). The diffraction is a natural property and it always present on any quasi-optical lens. Its effects may be masked if the lens has significant aberration. In the case of aspheric convex plano lenses, the diffraction is dominant over aberration. The diffraction-limited half-angle angular blur and corresponding circular ring of the diffraction pattern containing 86% of irradiance distribution, Fig. 3(b), is given as follows [22]:

$$\Delta\Theta_{\mathrm{diff}} = 1.64\frac{\lambda}{D}, \tag{8}$$

where $\lambda$ is the wavelength of MMW beam. The diffraction-limited blur spot size for finite conjugate ratio is given as [22]:

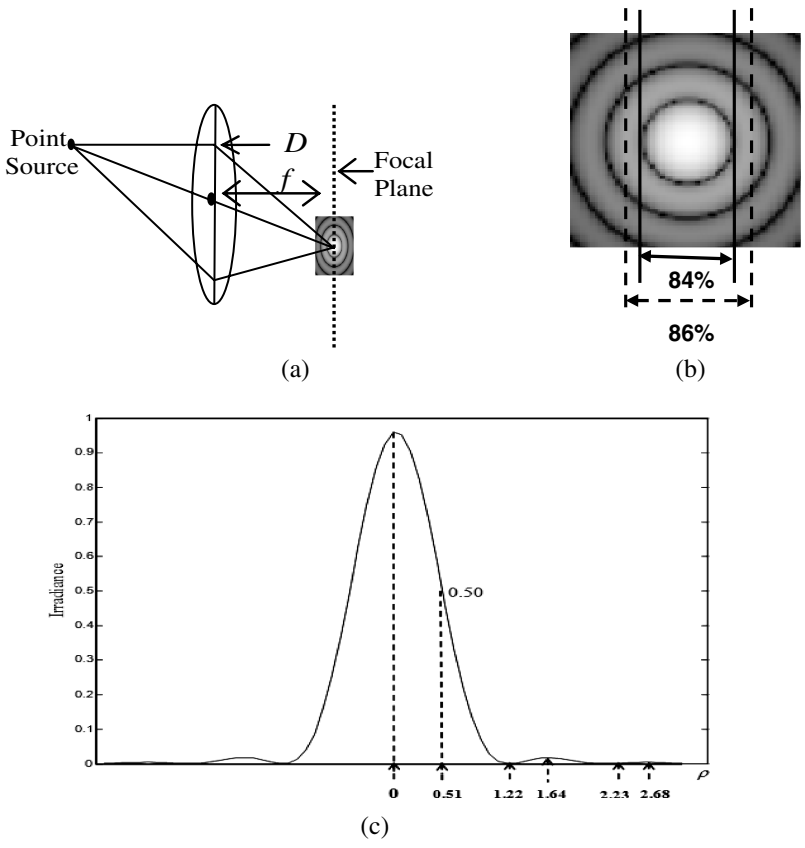


Fig. 3. (a) Image of a point object. (b) Airy pattern: 2-D plot of the diffracted irradiance distribution. (c) Cross-section of (b). $\rho$ is normalized radial distance from the center [22].

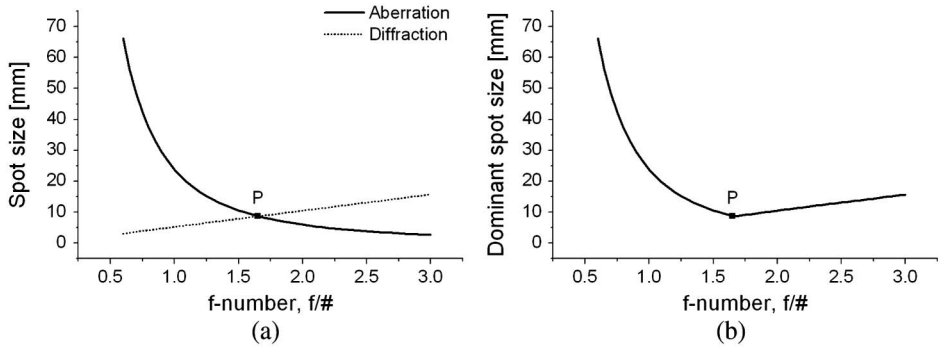


Fig. 4. (a) Aberration- and diffraction-limited and (b) dominant spot size of convex plano lens.

$$d_{\text{diff}} = \Delta\Theta_{\text{diff}} \cdot S_i = 1.64\lambda(M+1)f/\#. \tag{9}$$

The diffraction-limited blur spot size given by Eq. (9) is the radius of the circular ring of the diffraction pattern in the focal plane having 86% irradiance distribution [22].

Comparing the aberration-limited spot size to the diffraction-limited spot size suggests a criterion of a single lens. If the spot size $d_{ab}$ is larger than $d_{\text{diff}}$, then $d_{\text{blur}}$ is limited by aberration. If the spot size $d_{ab}$ is smaller than $d_{\text{diff}}$, the spot size is essentially diffraction limited. Figure 4 depicts the spot size as a function of $f/\#$ in the case of the convex-plane lens with the infinite conjugate ratio using Eqs. (7) and (9). Figure 4(a) shows that the spot size caused by spherical aberration is inversely dependent on the cube of $f/\#$ and the diffraction-limited spot size increases linearly with $f/\#$. The resultant spot size by the dominant fact decreases for small $f/\#$ and then increases with $f/\#$ as shown in Fig. 4(b). It means that there is some optimum point ($P$) for a minimum of both aberration and diffraction. The optimum spot size is about 8.7 mm at the $f/\#$ of 1.65 for the convex plano lens. The diffraction, a natural property, is always present on any quasi-optical lens, although its effects may be masked if the lens has a significant aberration. However, the spherical aberration can be reduced by aspherical lens or multiple lenses. Accordingly, an aspheric convex plano lens is mainly dominated by the diffraction and its focused beam spot diameter can be represented by the twice the diffraction-limited spot size given by Eq. (9).

In imaging applications, the SR is ultimately limited by diffraction. Calculating the maximum possible SR of a lens requires an arbitrary definition of what is meant by resolving two features. In the Rayleigh criterion, it is assumed that two separate point source can be resolved when the center of the Airy disc from one overlaps the first dark ring in the diffraction pattern of the second. In this case, the smallest resolvable distance is [22]:

$$r_{sp} = \frac{d_{\text{diff\_}o}}{2} = 1.22\lambda(M+1)f/\#, \tag{10}$$

where $d_{\text{diff\_}o}$ is the spot diameter at which the intensity distribution of the Airy disc is the first 0% intensity point of its maximum value on the axis for the finite conjugated lens. The SR is linearly proportional to $f/\#$ as shown in Eq. (10). It is also related to the physically minimum space between the adjacent receivers for a FPA imaging system.

The Gaussian beam focuses from a lens down to a waist and then expands proportionally to $x$ as shown in Fig. 5. The wavefront radius of curvature, which was infinite at $x = 0$, will become finite and initially decrease with $x$. At some point, it will reach a minimum value, and then it increases with larger $x$, eventually becoming proportional to $x$. The equations describing the Gaussian beam radius $w(x)$ and the wavefront radius of curvature $R(x)$ are [19,20]:

$$w(x) = w_o\left[1 + \left(\frac{\lambda x}{\pi w_o^2}\right)\right]^{0.5}, \tag{11}$$

$$R(x) = x\left[1 + \left(\frac{\pi w_o^2}{\lambda x}\right)^2\right], \tag{12}$$

where $x$ is the distance propagated from the plane where the wavefront is flat and $w_o = 0.5d_{\text{diff\_}o}$ is the radius of the $1/e^2$ irradiance contour at $x = 0$. The Rayleigh range, $X_R$, defined as the distance over the beam radius by a factor of $\sqrt{2}$, is given by [19,20]:

$$X_R = \frac{\pi w_o^2}{\lambda}. \tag{13}$$

DOF is the range of the image distance over which the focused spot diameter remains below an arbitrary limit. Normally, it is defined as the distance

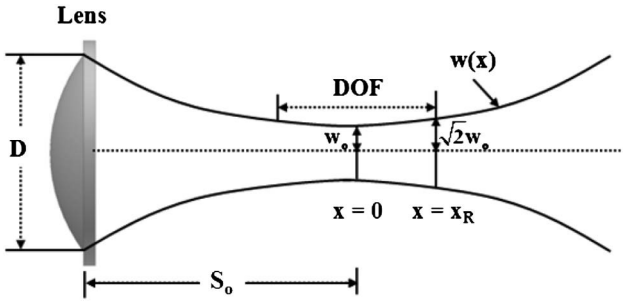


Fig. 5. Focusing of Gaussian beam.

Table 1. Theoretical Characteristics of Aspheric Lenses

| Characteristics | High $f/\#$ Lens($f/\# = 1.50$) | Low $f/\#$ Lens($f/\# = 0.93$) |
|---|---|---|
| $D$ [mm] | 350 | 350 |
| $S_i$ [mm] | 561 | 265 |
| $S_o$ [mm] | 2500 | 2500 |
| $F$ | 458 | 240 |
| $M$ | 0.22 | 0.11 |
| $f$-number | 1.3 | 0.7 |
| $d_{\text{blur}}$ [mm] | 8.4 | 4.0 |
| $r_{\text{sp}}$ [mm] | 6.2 | 3.0 |
| DOF [mm] | 76.6 | 17.3 |

between $\sqrt{2}w_o$ spot size points or 2 times Rayleigh range [19,20]. For the finite conjugated lens, it can be written as [19,20]:

$$\text{DOF} = 2 \times X_R = 2 \times \frac{\pi w_o^2}{\lambda} = 2.97\pi\lambda[(M+1)f/\#]^2. \quad (14)$$

It is clear from Eq. (14) that the DOF is proportional to the square of $f/\#$.

For the aspheric convex plano lens with two different $f/\#$, the main lens characteristics are calculated by using Eqs. (9), (10), and (14) and their values are summarized in Table 1. The quasi-optical lenses have the spot diameter of 8.4 and 4.0 mm, the SR of 6.2 and 3.0 mm, and DOF of 76.6 and 17.3 mm for high $f/\#$ and low $f/\#$, respectively. However, the real beam pattern of the low $f/\#$ lens may be relatively broad compared with the ideal pattern because the SR cannot be less than a wavelength, 3.2 mm. The theoretical results show that larger DOF requires larger $f/\#$ lens even though it leads to lower SR because of the larger focused beam.

### 3. Design of W-band Quasi-Optical Lens Antenna

The quasi-optics configuration, shown in Fig. 6, consists of a dielectric lens and a feed antenna. An aspheric convex plano lens type is selected for a quasi-optical lens in the W-band imaging system because of its advantages of low manufacturing cost and lower aberration-limited blurring than the spherical nonequiconvex and convex plano lens. We designed two aspheric convex plano lenses with aperture size

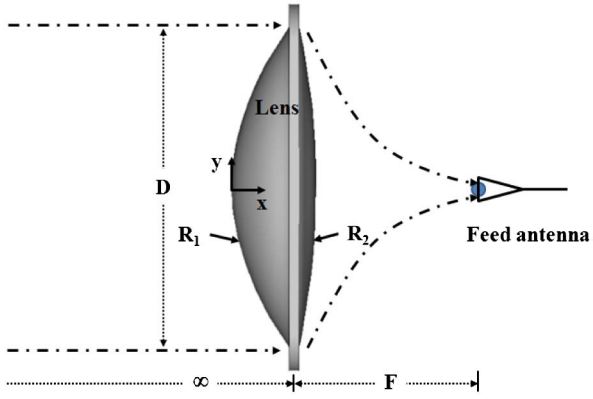


Fig. 6. (Color online) Configuration of quasi-optical lens antenna.

of 350 mm in the region band using the optics design tool CODE $V$ [23]. Equation (15) shows the design formula for the aspheric convex surface and it is based on the conic equation as follows:

$$y = \frac{x^2}{R\left(1 + \sqrt{1(1+k)x^2/R^2}\right)} + ax^4 + bx^6 + cx^8 + dx^{10}, \quad (15)$$

where $x$ and $y$ are the design coordinates of the lens surface. The high-order coefficients of the conic equation are $a$, $b$, $c$, and $d$. $R$ is the radius of the aspheric surface and $k$ is the conic constant. The constant values of the aspheric surface, described in Table 2, are optimized to achieve low spherical aberration. The designed two lenses have the different focal length with the same diameter to analyze the quasi-optical characteristics with respect to $f$-number, which is the ratio of the focal length over the diameter of the lens, $f/\# = F/D$. The focal lengths of the designed aspheric lenses with the lens diameter of 350 mm are 524 and 326 mm, corresponding to high $f/\#$ of 1.50 and low $f/\#$ of 0.93. The fabricated aspheric dielectric lenses are shown in Fig. 7. For low weight and low dissipation loss, the lenses are made of HDPE material with the refractive index of 1.5187 at 94 GHz [17,20].

As a feed antenna of quasi-optics in Fig. 6, the dielectric rod antenna (DRA) is adapted due to compact size and high gain compared with a standard waveguide type antenna in the MMW band. We designed DRA, which consists of a tapered dielectric rod and a WR-10 waveguide, for good quasi-optical transformation efficiency between a lens and a feed antenna using computer simulation technology microwave studio simulator [24]. The sharp dielectric rod of DRA is made of acrylonitrile butadiene styrene material with refractive index of 1.6105 at 94 GHz [17] because this material is harder than HDPE used for DRA in [25]. The fabricated DRA, shown in Fig. 8, is the total length of about 30 mm. The return loss and radiation pattern of DRA, as shown in Figs. 9(a) and 9(b), are measured by HP 8510 vector network analyzer and near-field measurement equipment. The return loss is below −15 dB over the full W-band and the H-plane radiation pattern has a gain of about 15.3 dB, the first side lobe level of below −20 dB, and 10 dB beam widths of about 51.1° at 94 GHz.

Table 2. Designed Constants of Aspheric Lenses

| Constant | High $f/\#$ Lens ($f/\# = 1.50$) | Low $f/\#$ Lens ($f/\# = 0.93$) |
|---|---|---|
| $R$ | 271.847 | 168.998 |
| $k$ | −0.184 | −5.761 |
| $a$ | −2.056e−9 | −1.123e−7 |
| $b$ | −5.852e−14 | 4.229e−12 |
| $c$ | 1.458e−18 | −1.123e−16 |
| $d$ | −2.625e−23 | 1.189e−21 |

(a) (b)

Fig. 7. (Color online) Photo of fabricated aspheric lenses with (a) high $f/\#$ and (b) low $f/\#$ (Courtesy Millisys Inc.).

## 4. Measurement and Optical Performance Analysis of Quasi-Optical Lens Antenna

The validation of the quasi-optical characteristics via $f$-number of a lens is implemented in component-level and system-level test. The test is mainly focused on measuring the main characteristics, such as focal length, DOF, beam spot size, and SR of two manufactured lenses.

The component-level test is used to verify all of lens characteristics by measuring Gaussian beam pattern of a lens. Figure 10 shows the experimental setup for component-level test of a lens [17]. A W-band source and a DRA are applied as a transmitter. A W-band power meter was attached to a DRA as a receiver antenna to measure the received power. To test the focal length and DOF of the designed quasi-optical lenses, the receiver was scanned on the optical axis by scan step size of 1 mm to measure the received power through the image distance, $S_i$, at the fixed object distance, $S_o = 2500$ mm. In this test setup, the optimum image distance is the space from the lens to the receiver when the maximum output power of the receiver was observed. The experimental focal length and DOF of the lenses can be calculated by using Eq. (1) and by computing −3 dB level ranges where the received power is 3 dB lower than the maximum power at the optimum image distance. For test of the beam spot size and SR of the lenses, the receiver was horizontally scanned on the origin of the optimum image distance by scan step size of 0.5 mm to measure the focused beam pattern on H-plane at $S_o = 2500$ mm. We can get the experimental beam spot diameter and SR of the lenses by using −8.6 dB level ranges and first inflection point from the maximum power point of the measured beam pattern.

Fig. 8. (Color online) Fabricated DRA (Courtesy Millisys Inc.).

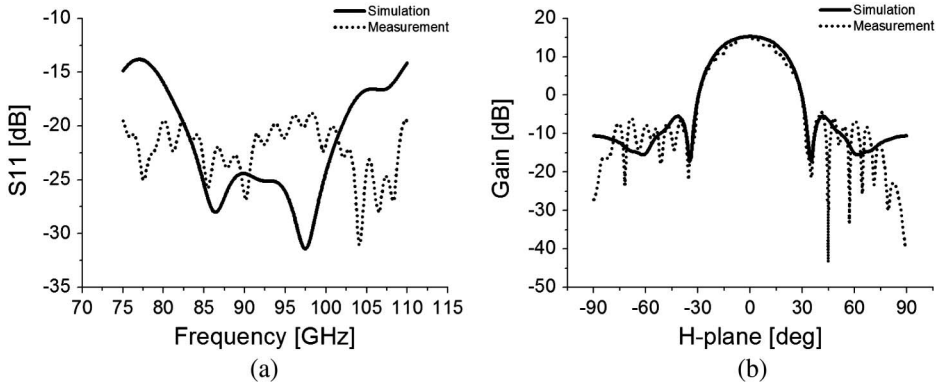


Fig. 9. Measurement results of DRA: (a) return loss and (b) H-plane radiation pattern.

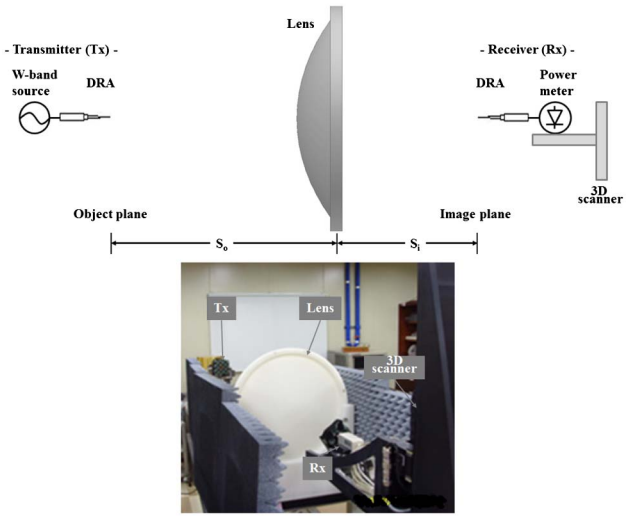


Fig. 10. (Color online) Experimental setup of aspheric lens in component-level.

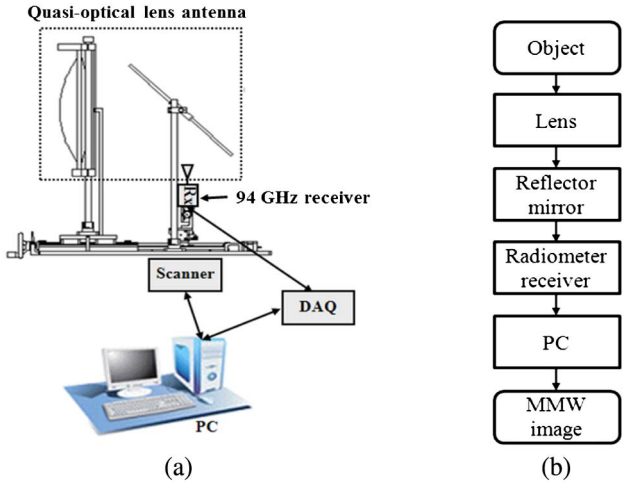


Fig. 13. (Color online) (a) Configuration and (b) signal flow of 94 GHz radiometer imaging system.

As for the results of component-level test, the Gaussian propagation beam pattern at 94 GHz via image distance is depicted in Fig. 11 for two different $f/\#$ lenses. As shown in Fig. 11(a), the image distance $S_i = 561$ mm, of the high $f/\#$ lens is measured at $S_o = 2500$ mm. According to the distance information, the focal length, $F$, of about 458 mm can be calculated by using Gaussian lens formula. The DOF, of −3 dB ranges is around 65 mm. As shown in Fig. 11(b), the measured image distance of the low $f/\#$ lens is $S_i = 265$ mm at $S_o = 2500$ mm. This leads to a focal length of approximately 240 mm and DOF of about 23 mm. Further, the object distance is set by 2500 mm and then the measurement of the focused H-plane beam patterns of the quasi-optical lenses on the image plane are performed at three different frequencies of 90, 94, and 100 GHz. As depicted in Fig. 12, the focused H-plane beam patterns for each high $f/\#$ and low $f/\#$ lens are very similar at all frequencies. The beam diameters at −8.6 dB point are about 9.4 and 7.5 mm at 94 GHz for two

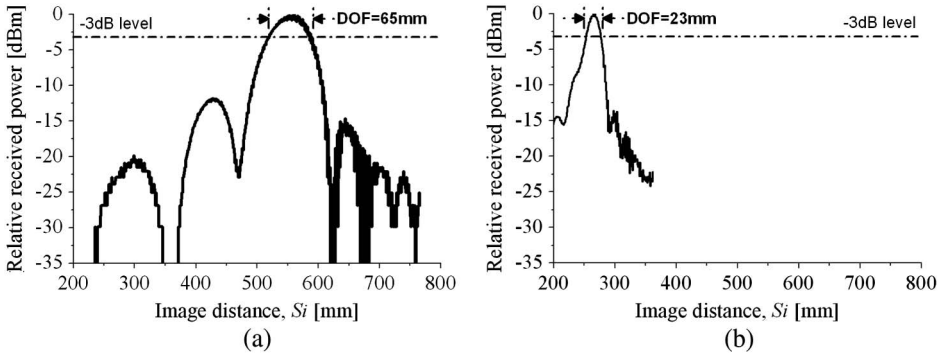


Fig. 11. Received power via image distance for (a) high $f/\#$ and (b) low $f/\#$ lens at 94 GHz.

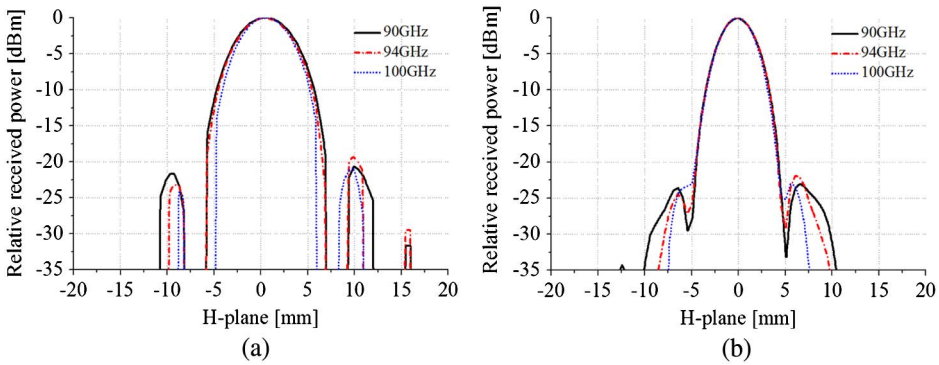


Fig. 12. (Color online) H-plane focused beam pattern of (a) high $f/\#$ and (b) low $f/\#$ at $S_o = 2500$ mm.

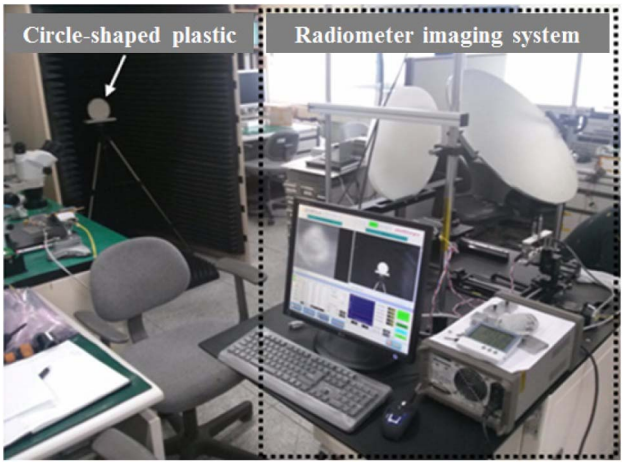


Fig. 14. (Color online) Experimental setup of aspheric lens in system-level test.

quasi-optical lenses. The results of the component-level test demonstrate that larger $f/\#$ of a lens leads to larger DOF, although it induces larger beam spot size and lower SR.

The DOF can be also measured through system-level test using a W-band radiometer imaging system whose configuration and signal flow are shown in Fig. 13. The fabricated 94 GHz system consists of quasi-optical lens antenna with a reflector mirror, radiometer receiver, scanner, and PC with a DAQ. The performance of the imaging system are temperature sensitivity of below 1 K [17], SR of about 0.64°, and FOV of above $10° \times 10°$ in W-band. Figure 14 shows the experimental setup for the system-level test of a quasi-optical lens. The manufactured radiometer imaging system is used to measure DOF of two designed quasi-optical lenses by getting W-band radiometer images depending on the image distance

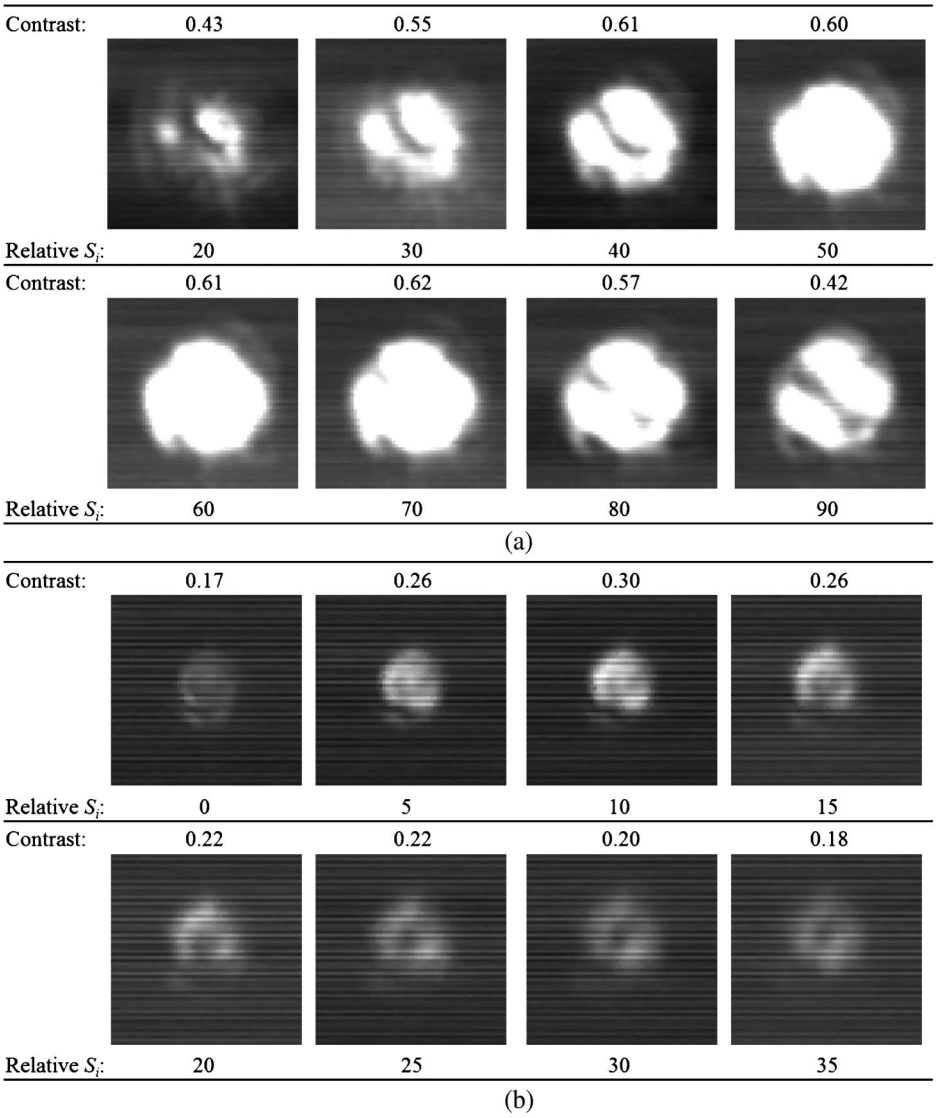


Fig. 15. Measured images and relative IC via image distance for (a) high and (b) low $f/\#$ lens.

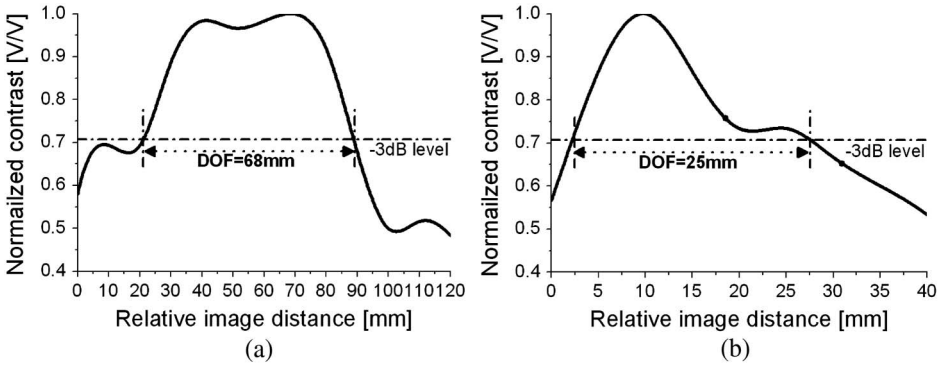


Fig. 16. Normalized IC via relative image distance for (a) high $f/\#$ lens and (b) low $f/\#$ lens.

at the fixed object distance $S_o = 2500$ mm. The DOF is the image distance ranges where the acceptable sharpness image is achieved. It can be represented by image contrast (IC), which is given by

$$\mathrm{IC} = \frac{\text{Voltage amplitude}}{\text{Voltage average}} = \frac{V_{\max} - V_{\min}}{V_{\max} + V_{\min}}[V/V], \quad (16)$$

where $V_{\max}$ and $V_{\min}$ are the maximum and minimum output voltage of the receiver within a radiometer image frame. The DOF is the range between 0.707 points of IC via the image distance. The circle-shaped Teflon plastic positioned at 2.5 m from the lens is used as a target and it is surrounded by absorber sheets to reduce the effects of environmental clutters on the image. The measured images and IC for each image are shown in Fig. 15. The IC via the relative image distance are first normalized by the maximum value and then interpolated due to wide step size compared with that of the component-level test. The experimental DOF in the system-level test are 68 and 25 mm for high $f/\#$ and low $f/\#$ lens, as shown in Fig. 16. The results are very similar to that of the component-level test.

All measurement data of the two lenses are summarized in Table 3. The measurement results show that if the lens has higher $f/\#$, the lens will be larger SR and depth of field. The experimental results and trends are very well-matched with the theoretical outcomes. However, the difference between two data can be caused by the difficulty to know exactly the electrical characteristics of HDPE material used at 94 GHz and the manufacturing error of the large aperture aspheric lens. In addition, the experimental limitations, such as alignment and step size between test points, causes the difference, especially more critical for low $f/\#$ lens because of the relationship between the lens characteristic and $f/\#$.

**Table 3. Experimental Results of Aspheric Lenses at 94 GHz**

| Characteristics | High $f/\#$ Lens ($f/\# = 1.50$) | Low $f/\#$ Lens ($f/\# = 0.93$) |
|---|---|---|
| $D$ [mm] | 350 | 350 |
| $S_i$ [mm] | 561 | 265 |
| $S_o$ [mm] | 2500 | 2500 |
| $F$ | 458 | 240 |
| $M$ | 0.22 | 0.11 |
| $f/\#$ | 1.3 | 0.7 |
| $d_{\mathrm{blur}}$ [mm] | 9.4 | 6.3 |
| $r_{\mathrm{sp}}$ [mm] | 6.7 | 5.0 |
| DOF [mm] (component/system) | 65/68 | 23/25 |

## 5. Conclusion

The quasi-optical characteristics via $f/\#$ are theoretically and experimentally analyzed in a MMW imaging system. Two low aberration aspheric convex plano lenses are designed at 94 GHz and the lenses have a diameter of 350 mm and different $f/\#$ of 1.3 and 0.7. The experimental results show that the averaged DOF is 66 and 24 mm and the SR is 6.7 and 5.0 mm for high $f/\#$ and low $f/\#$ lens. It is conformed that the large $f/\#$ lens gives large DOF to the quasi-optical imaging system. The proper $f/\#$ of a lens should be selected to complete sharpness image for a FPA imaging system because there is a tradeoff between the DOF and the SR. This result can be used as an important design guideline of the quasi-optical lens antenna for the MMW imaging system with lower SR compared to IR cameras.

The work was supported by the basic research program from the Agency for Defense Development (ADD) and by the BK21 program at Gwangju Institute of Science and Technology in the Republic of Korea. All radiometer hardware was manufactured and supported by Millisys Inc. (http:www.millisys.com).

## References

1. J. P. Samluk, C. A. Schuetz, T. Dillon, E. L. Stein, A. Robbins, D. G. Mackrides, R. D. Martin, J. Wilson, C. Chen, and D. W. Prather, "Q-band millimeter wave imaging in the far-field enabled by optical upconversion methodology," J. Infrared Millimeter Terahertz Waves **33**, 54–66 (2012).
2. S. Yeom, D. S. Lee, J. Y. Son, M. K. Jung, Y. Jang, S. W. Jung, and S. J. Lee, "Real-time outdoor concealed-object detection with passive millimeter wave imaging," Opt. Express **19**, 2530–2536 (2011).
3. J. J. Lynch, P. A. Macdonald, H. P. Moyer, and R. G. Nagele, "Passive millimeter wave imaging sensors for commercial markets," Appl. Opt. **49**, E7–E12 (2010).

4. C. F. Cull, D. A. Wikner, J. N. Mait, M. Mattheiss, and D. J. Brady, "Millimeter-wave compressive holography," Appl. Opt. **49**, E67–E82 (2010).
5. S. Y. Li, B. L. Ren, H. J. Sun, W. D. Hu, and X. Lv, "Modified wavenumber domain algorithm for three-dimensional millimeter-wave imaging," Prog. Electromagn. Res. **124**, 35–53 (2012).
6. F. Gumbmann and L. P. Schmidt, "Millimeter-wave imaging with optimized sparse periodic array for short-range applications," IEEE Trans. Geosci. Remote Sens. **49**, 3629–3638 (2011).
7. K. Haddadi, D. Glay, and T. Lasri, "A 60 Ghz scanning near-field microscope with high spatial resolution sub-surface imaging," IEEE Microw. Wireless Compon. Lett. **21**, 625–627 (2011).
8. F. Qi, V. Tavakol, I. Ocket, P. Xu, D. Schreurs, J. K. Wang, and B. Nauwelaers, "Millimeter wave imaging system modeling: spatial frequency domain calculation versus spatial domain calculation," J. Opt. Soc. Am. A **27**, 131–140 (2010).
9. N. N. Wang, J. H. Qiu, P. Y. Zhang, and W. B. Deng, "Passive millimeter wave focal plane array imaging technology," J. Infrared Millimeter Waves **30**, 419–424 (2011).
10. E. L. Jacobs and O. Furxhi, "Target identification and navigation performance modeling of a passive millimeter wave imager," Appl. Opt. **49**, E94–E105 (2010).
11. F. Qi, V. Tavakol, D. Schreurs, and B. Nauwelaers, "Limitations of approximations towards Fourier optics for indoor active millimeter wave imaging systems," Prog. Electromagn. Res. **109**, 245–262 (2010).
12. F. Hu and Y. Feng, "Passive millimeter wave focal plane imaging method combined with interferometry," J. Infrared Millimeter Waves **28**, 382–385 (2009).
13. A. Rolland, M. Ettorre, A. V. Boriskin, L. Le Coq, and R. Sauleau, "Axisymmetric resonant lens antenna with improved directivity in Ka- band," IEEE Antennas Wireless Propag. Lett. **10**, 37–40 (2011).
14. Z. X. Wang and W. B. Dou, "Full-wave analysis of monopulse dielectric lens antennas at W-band," J. Infrared Millimeter Terahertz Waves **31**, 151–161 (2010).
15. B. Fuchs, R. Golubovic, A. K. Skrivervik, and J. R. Mosig, "Spherical lens antenna designs with particle swarm optimization," Microw. Opt. Technol. Lett. **52**, 1655–1659 (2010).
16. A. H. Lettington, D. Dunn, M. Attia, and I. M. Blankson, "Passive millimetre-wave imaging architectures," J. Opt. A **5**, S103–S110 (2003).
17. W. G. Kim, N. W. Moon, J. M. Kang, and Y. H. Kim, "Loss measuring of large aperture quasi-optics for W-band imaging radiometer system," Prog. Electromagn. Res. **125**, 295–309 (2012).
18. C. D. Meinhart and S. T. Wereley, "The theory of diffraction-limited resolution in microparticle image velocimetry," Meas. Sci. Technol. **14**, 1047–1053 (2003).
19. Technical guide on fundamental optics, http://www.cvimellesgriot.com/.
20. P. F. Goldsmith, *Quasi-optical Systems: Gaussian Beam Quasi-optical Propagation and Applications*, 4th ed. (IEEE, 1998).
21. Technical document about lens theory from http://www.lasercomponents.com/de/.
22. G. D. Boreman, *Modulation Transfer Function in Optical and Electro-Optical Systems* (SPIE, 2001).
23. http://www.opticalres.com/.
24. http://www.cst.com/.
25. K. W. Gyum, J. P. Thakur, and Y. H. Kim, "Efficient DRW antenna for quasi-optics feed in W-band imaging radiometer system," Microw. Opt. Technol. Lett. **52**, 1221–1223 (2010).